Contents lists available at ScienceDirect

Arabian Journal of Chemistry

journal homepage: www.ksu.edu.sa

Original article

In-situ synthesis of fluorine-free MXene/TiO_2 composite for high-performance supercapacitor

Kefeng Xie [a,*], Jie Wang [a], Kai Xu [a], Zheng Wei [b], Mingli Zhang [b,*], Junping Zhang [b,*]

[a] School of Chemistry and Chemical Engineering, Lanzhou Jiaotong University, Lanzhou 730070, China
[b] Henan Academy Institute of Traditional Chinese Medicine, Zhengzhou 45000, China

ARTICLE INFO

Keywords:
MXene
Fluorine-free
TiO_2
In-situ Synthesis
Supercapacitor

ABSTRACT

MXene ($Ti_3C_2T_x$) is a promising electrode material for supercapacitors. However, the current MXene material preparation process often requires hydrofluoric acid, and the etched MXene is easily oxidized and stacked, which is not conducive to the transfer of electrons and ions. In this study, we proposed a high concentration of sodium hydroxide solution mixed with sodium hypochlorite solution as an etchant for the preparation of fluorine-free MXene ($Ti_3C_2T_x$). Based on the alkali-assisted hydrothermal method, Ti_3AlC_2 was used as the raw material, and 10 % NaClO aqueous solution was added as the oxidant during the etching process to accelerate the etching and in-situ generate TiO_2 with excellent conductivity. When the oxidation time is 12 h and the amount of NaClO is 0.2 mL, the TiO_2 particles in-situ generated by the oxidation of Ti element in MXene are evenly distributed on the surface and interlayer of the material, which effectively curbs the stacking problem between the $Ti_3C_2T_x$ layers and improves the specific surface area of the material. The prepared MXene/TiO_2 electrode in 1 M H_2SO_4 electrolyte, − 0.5–0.2 V voltage window, the highest mass specific capacity can reach 321F/g, and after 10,000 charge–discharge cycles, the capacitance retention rate can still reach 86.4 %, which is higher than the capacitance retention rate of $Ti_3C_2T_x$ material (81.7 %).

1. Introduction

With the aggravation of various environmental problems such as the depletion of fossil energy, the public's voice for new energy is becoming stronger. In the context of vigorously developing green energy, energy storage devices have become a hot research topic, among which supercapacitors (SCs) and lithium-ion batteries (LiBs) are two typical representatives (Yang et al., 2023; Fei et al., 2023; Wodyk et al., 2023; Abdalla et al., 2023). Compared with LiBs, SCs have the characteristics of high-power density, fast charge and discharge speed (Sun and Bi, 2012; Grygorchak et al., 2019), and long service life (An et al., 2023, 2023; Cao et al., 2023; An et al., 2020). Supercapacitors are usually divided into two types: electric double-layer capacitors (EDLCs) (Seo et al., 2023; Tovar-Martinez et al., 2023; Hung et al., 2022; Sun et al., 2022) and pseudocapacitors (Mahala et al., 2023; Lichchhavi et al., 2023; Ahn et al., 2023; Chen et al., 2023; Qu et al., 2022). Among them, the energy density of pseudocapacitors based on surface Faraday storage is much higher than that of double-layer capacitors that store electrical energy by electrostatic accumulation of charges along the electrode interface (Liu et al., 2022; Zhao et al., 2022; Sun et al., 2023; Zhao et al., 2023). The development of pseudocapacitive materials with high capacitance can improve the energy density of supercapacitors. Pseudocapacitive materials include MXene (Ye et al., 2023; Zheng et al., 2022; Das and Majumdar, 2022; Panda et al., 2022), TiO_2 (Lakra et al., 2023; Simon et al., 2023; Waris et al., 2023; Zhang et al., 2017); RuO_2 (Thangappan et al., 2018; Grover et al., 2023; Manuraj et al., 2020; Karimi et al., 2022), MnO_2 (Han et al., 2020; Xiao et al., 2020; Bagal et al., 2021; Chowdhury et al., 2023), and so on.

MXene is a new type of two-dimensional transition metal carbide/carbonitride. It is favored by many researchers because of its excellent electrical conductivity, rich surface functional groups, good mechanical properties and unique hydrophilicity. $Ti_3C_2T_x$(MXene) is synthesized by etching the Al element in Ti_3AlC_2 with HF (Naguib et al., 2011). In this process, the presence of fluoride leads to the production of byproducts with certain risks, including toxic gases, intercalated water and filtered wastewater. So researchers have used NH_4HF_2 (Halim et al., 2014), dilute HCl and LiF instead of HF to improve the synthesis condition (Natu et al., 2020). Moreover, fluorine-free $Ti_3C_2T_x$ is prepared by alkali-assisted hydrothermal method with high concentration NaOH solution, which has 314F/ g via gravimetric capacitance (Li et al., 2018).

* Corresponding authors.
E-mail addresses: xiekefeng@mail.lzjtu.cn (K. Xie), zhang120@126.com (M. Zhang), zhangjunping@hactcm.edu.cn (J. Zhang).

https://doi.org/10.1016/j.arabjc.2023.105551
Received 30 June 2023; Accepted 11 December 2023
Available online 12 December 2023

However, there are few active sites on the surface of MXene, and the layered single-layer or few-layer nanosheets are prone to agglomeration, resulting in a decrease in specific surface area and a decrease in electrical properties.

Metal oxide is considered as efficient electrodes for supercapacitors due to their excellent electrochemical properties (Lv et al., 2023). To improve the capacitance, power density, cycle efficiency and cycle life of supercapacitors, researchers have done a lot of work (Khajonrit et al., 2022; Zhang et al., 2022; Chen, 2021; Liu et al., 2022; Zhang et al., 2021; Zeng et al., 2022). However, various parameters need to be considered to improve the performance, such as the specific surface area of the electrode material, the selection of high-performance materials, preparation/synthesis technology and the active life of the material. TiO_2 has received extensive attention in supercapacitor energy storage systems due to its advantages of easy availability, low-cost, high-energy density, non-toxicity, and chemical stability. Even after 50,000 cycles at a very high energy density, the TiO_2-based electrode can still maintain 95 % cycle efficiency (Gao et al., 2015; Li et al., 2021). He et al. developed TiO_2 nanotube arrays (NTA) as a current collector for supercapacitors (He et al., 2021). Among them, MnO_2-modified TiO_2 NTA as the cathode showed an extremely high capacitance value (1051F/cm^3), while the volume capacitance of Fe_2O_3 with TiO_2 NTA as the anode reached 608.2F/cm^3, and the asymmetric supercapacitor based on the electrode retained about 91.7 % of the capacitance after 5000 cycles. The hydrothermal method is an effective method to synthesize metal oxide nanoparticles for supercapacitors (Wu et al., 2014).

To make TiO_2-based binary and ternary composites become high-performance supercapacitor electrode materials, many researchers have tried to use them as electrode materials. In this study, Ti_3AlC_2 was used as the raw material, and 10 % NaClO aqueous solution was added as the oxidant during the etching process to accelerate the etching and in-situ generate fluorine-free $Ti_3C_2T_x/TiO_2$ composite based on the alkali-assisted hydrothermal method. The structure and electrochemical properties of fluorine-free $Ti_3C_2T_x/TiO_2$ composite were studied in detail.

2. Experimental procedure

2.1. Synthesis of MXene/TiO_2 materials

The key parameters of the preparation process of MXene/TiO_2 composite, reaction time and the amount of NaClO, were optimized in Fig. S1. The optimal MXene/TiO_2 was studied in paper. The preparation method of a fluorine-free MXene/TiO_2 material was alkali-assisted hydrothermal method, using 10 % NaClO solution and Ti_3AlC_2 powder as raw materials. The preparation process by adjusting the reaction time and the amount of NaClO added was shown in Fig. 1. The optimal solution is: 200 mg Ti_3AlC_2 powder was weighed. 27.5 g NaOH was weighed, and 25 mL NaOH solution was taken after NaOH was fully dissolved with 50 mL deionized water. 0.02 mL of 10 % NaClO aqueous solution was taken by pipette, and the above drugs were added to the high-pressure reactor, sealed after N_2, and heated for 12 h in the electric blast drying box at 270 °C. After the reaction, the bottom precipitate was washed out and stood for 30 min. The upper suspension after standing was poured and water was added for ultrasound (power: 100 %, time: 30 min). At the end of ultrasound, the solution was centrifuged (time: 5 min). After centrifugation, the pH value of the supernatant was detected, washed, and centrifuged until the pH value of the upper suspension was 6.5, and the bottom precipitate was washed with 95 % ethanol solution. The bottom precipitate was washed out and poured into a conical flask, and a well-balanced 24 mL DMSO solution was poured into a fume hood, and placed on a magnetic heating stirrer to stir for intercalation and delamination (time: 24 h); after the intercalation, the upper layer of DMSO was poured and immersed in deionized water for 12 h. The soaked solution was subjected to ultrasonic treatment for 1 h. The ultrasonic suspension was centrifuged (speed: 4000 rpm, time: 10 min), and the upper solution after centrifugation was observed. If it showed dark green, the ultrasound was stopped, otherwise the above ultrasound and centrifugation were repeated. The bottom precipitate was washed out with 95 % ethanol, and the obtained sample was dried in a vacuum oven at 50 °C for more than 48 h to obtain the target product $Ti_3C_2T_x/TiO_2$.

2.2. Characterization method

The surface morphology of the material was scanned by the focused electron beam in the scanning electron microscope (SEM). During the sample preparation, a small amount of powder was placed on the conductive adhesive using a toothpick, and dried by a blower after leveling and spreading. The SEM was performed on the GeminiSEM500 electron microscope of ZEISS. The elemental composition and content of the material were preliminarily determined by point or surface analysis using energy dispersive spectroscopy (EDS), which was used in conjunction with SEM. The transmission electron microscope (TEM) was performed on JEOL JEM-F200. The specific surface area was determined by Micromeritics ASAP 2460. The crystal structure and elemental composition of the material were analyzed by Japanese Rigaku MiniFlex600 X-ray diffractometer (XRD), and the scanning angle range was 5°-90°. The composition of the material was qualitatively analyzed using Thermo Scientific K-Alpha X-ray spectrometer (XPS) for full-spectrum scanning (energy 100 eV, step size 1 eV) and narrow-spectrum scanning (energy 50 eV, step size 0.1 eV). The charge correction was performed with C 1 s = 284.80 eV binding energy as the energy standard.

2.3. Electrochemical test

The fluorine-free $Ti_3C_2T_x/TiO_2$ composite material was made into a working electrode: 4 mg $Ti_3C_2T_x/TiO_2$ and 0.7 mg acetylene black were

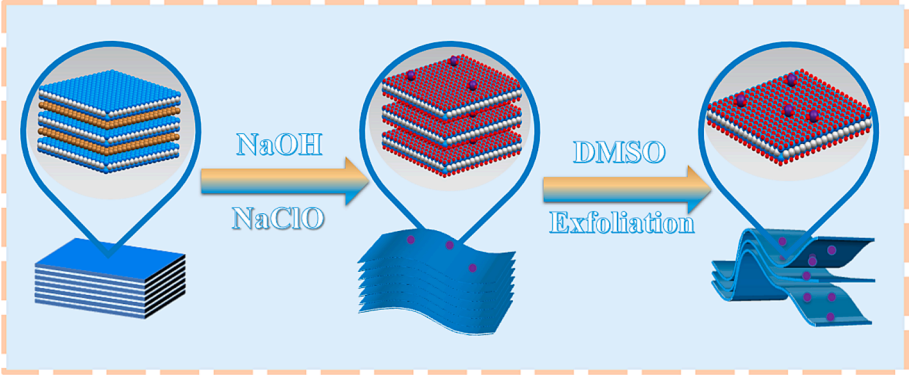

Fig. 1. Preparation process of fluorine-free $Ti_3C_2T_x$ / TiO_2 composite.

weighed and ground in agate mortar for 5–10 min; the milled mixed material was scraped into the sample bottle, and 0.4 mL perfluorosulfonic acid solution (Nafion) was added and sonicated for 25–30 min to make the powder and Nafion solution mixed evenly. A 6 μL uniformly dispersed solution was absorbed by a pipette and dropped onto the working electrode for testing. The electrode material loading was 6×10^{-5} g. The tester is Shanghai Chenhua's CHI660E electrochemical workstation, using the traditional three-electrode system, the electrolyte is 1 M H_2SO_4, the reference electrode and the counter electrode in the system are calomel electrode and carbon rod respectively. Electrochemical performance tests mainly include cyclic voltammetry (CV), constant current charge and discharge (GCD), electrochemical impedance spectroscopy (EIS) and cycle stability. Cyclic voltammetry was performed in the voltage range (−0.5—0.2 V) at scan rates of 10, 20, 30, 50, 100, 200 mV/s, respectively.

The specific capacitance of the material can be calculated by the CV curve. The calculation formula is shown in (1):

$$C_m = \frac{\int idV}{2vm\Delta V} \tag{1}$$

Among them, C_m is the specific capacitance of the material (F/g), i is the discharge current (A), v is the voltage scanning rate (V/s), m is the mass of the active material loaded on the electrode (g), and ΔV is the discharge voltage (V).

The specific capacitance of the material can also be calculated by the GCD curve. The calculation formula is shown in (2):

$$C_m = \frac{i\Delta t}{m\Delta V} \tag{2}$$

Among them, C_m is the specific capacitance of the material (F/g), i is the discharge current (A), Δt is the discharge time (s), m is the mass of the active material loaded on the electrode (g), and ΔV is the potential window (V).

3. Results and discussion

3.1. Characterization and analysis of material structure

$Ti_3C_2T_x/TiO_2$ composites was prepared by 0.2 mL 10 % NaClO aqueous solution were characterized by SEM and TEM. The morphology of $Ti_3C_2T_x/TiO_2$ composites taken from different angles was not difficult to find that the high concentration NaOH solution selected in this experiment successfully peels the Al atomic layer from the Ti_3AlC_2 powder in the high temperature and high-pressure environment, and the final $Ti_3C_2T_x$ material showed good morphology in Fig. 2 (a-c). EDS elemental analysis was performed on $Ti_3C_2T_x/TiO_2$ composites with excellent morphology (0.2 mL NaClO aqueous solution). Fig. 2a showed that there were many granular materials on the surface and between the layers of $Ti_3C_2T_x/TiO_2$ composites. After etching with NaOH and NaClO solution, a large number of TiO_2 particles were attached to the surface and interlayer of the composite material, which played a role in expanding the interlayer spacing, reducing the stacking effect and endowing the material with more excellent pseudocapacitance. In addition, the expansion of the interlayer spacing increaseed the effective contact area between the electrode and the electrolyte, thereby improving the electrochemical performance of the composite. The red box in the figure was the mapping scanning position, and the Fig. 2 (d-f) was the EDS mapping image of the main elements of Ti, C and O. In addition, the crystal structure of the prepared samples was analyzed by XRD. Fig. 2g was the XRD spectra of $Ti_3C_2T_x$, and $Ti_3C_2T_x/TiO_2$ composites. Compared with the standard comparison card of $Ti_3C_2T_x$ (PDF#52–0875) and the $Ti_3C_2T_x$ material prepared without adding oxidant, the diffraction peaks at 37.8°, 48.1° and 62.1° in the spectrum of the composite material correspond to the anatase TiO_2 (004), (200) and (213) crystal planes, respectively. The peak of $Ti_3C_2T_x$ itself weakens and widens. The reason was that the strong oxidant destroys the crystal structure of the material during the etching process, reduces the crystallinity, and the material was oxidized to TiO_2.

The specific surface area significantly affected the capacitance of the material. An increase in specific surface area resulted in a greater number of surface-active sites, which promoted the capacitance. BET of N_2 adsorption–desorption isotherms, and pore size distribution of MXene and MXene/TiO_2 showed in Fig. 3. The specific surface area of MXene was 3.47 m^2/g, however, that of MXene/TiO_2 was 14.21 m^2/g. This enhanced specific surface area increased the capacitance by increasing the quantity of surface-active sites (Fig. 3a). Furthermore, MXene/TiO_2 exhibited a micropore structure (Fig. 3b). Hence, the increase in the specific surface area of MXene/TiO_2 was attributed to the formation of a more intricate pore structure with a high pore volume.

$Ti_3C_2T_x/TiO_2$ composites were characterized by XPS. Fig. 4a was the spectrum of the composite, where the peaks of C, O and Ti in $Ti_3C_2T_x$ could be found. Through the peak fitting of each element in the composite material, the element distribution in the material can be effectively understood. Fig. 4b was the fitted C peak. The binding energies of C-Ti, C-O, C–C and C = O were 280.8 eV, 284.2 eV, 284.8 eV and 288.1 eV, respectively. Ti 2p spectra of Fig. 4c corresponded to Ti-C ($2p_{3/2}$), Ti-O ($2p_{3/2}$), Ti-C ($2p_{1/2}$) and Ti-O ($2p_{1/2}$) bonds at 455.6 eV, 458.3 eV, 461 eV and 464.5 eV, respectively. As shown in Fig. 4d, the binding energies of O-Ti, O = C and O-C bonds were 529.7 eV, 531.5 eV and

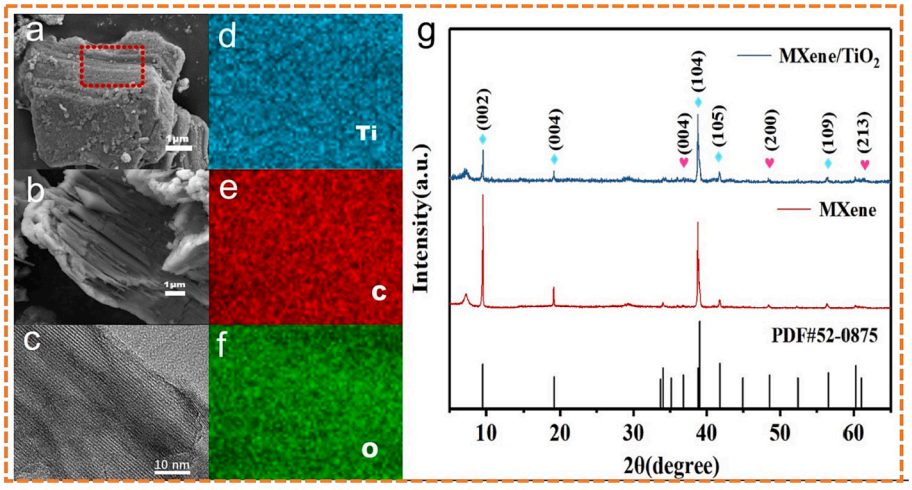

Fig. 2. (a-c) are the overall SEM and TEM image of fluorine-free $Ti_3C_2T_x$ doped with 0.2 mL 10 % NaClO at different angles; (d-f) are the element mapping figure of Ti, C and O in $Ti_3C_2T_x/TiO_2$ composites; (g) is the XRD spectrum of the material.

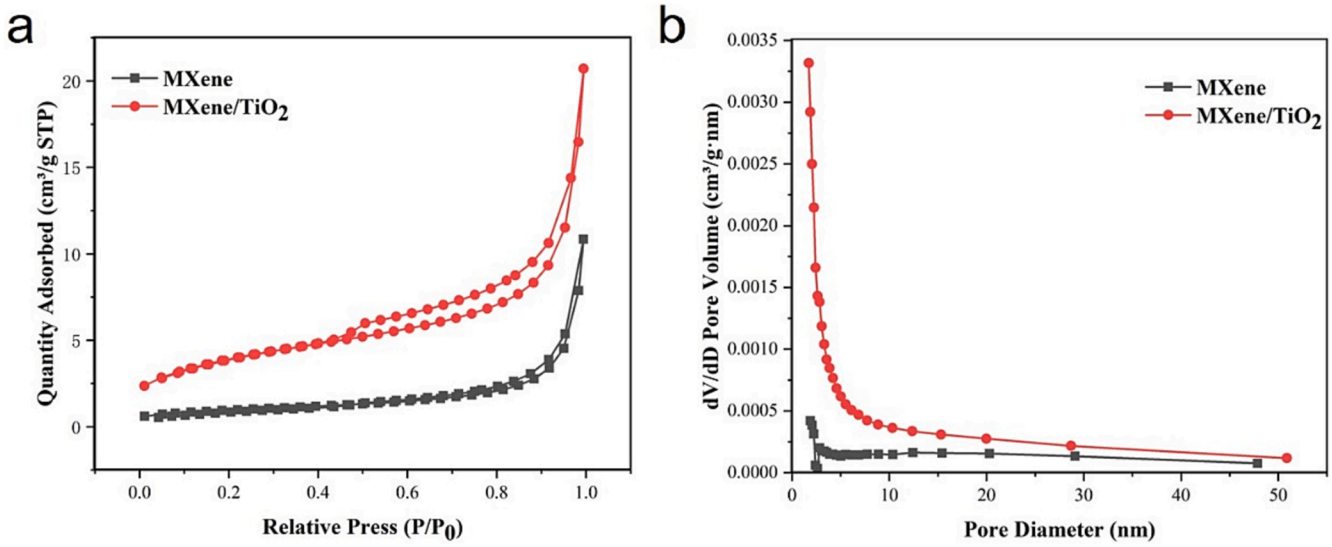

Fig. 3. BET of N_2 adsorption–desorption isotherms (a), and pore size distribution of MXene and MXene/TiO_2 (b).

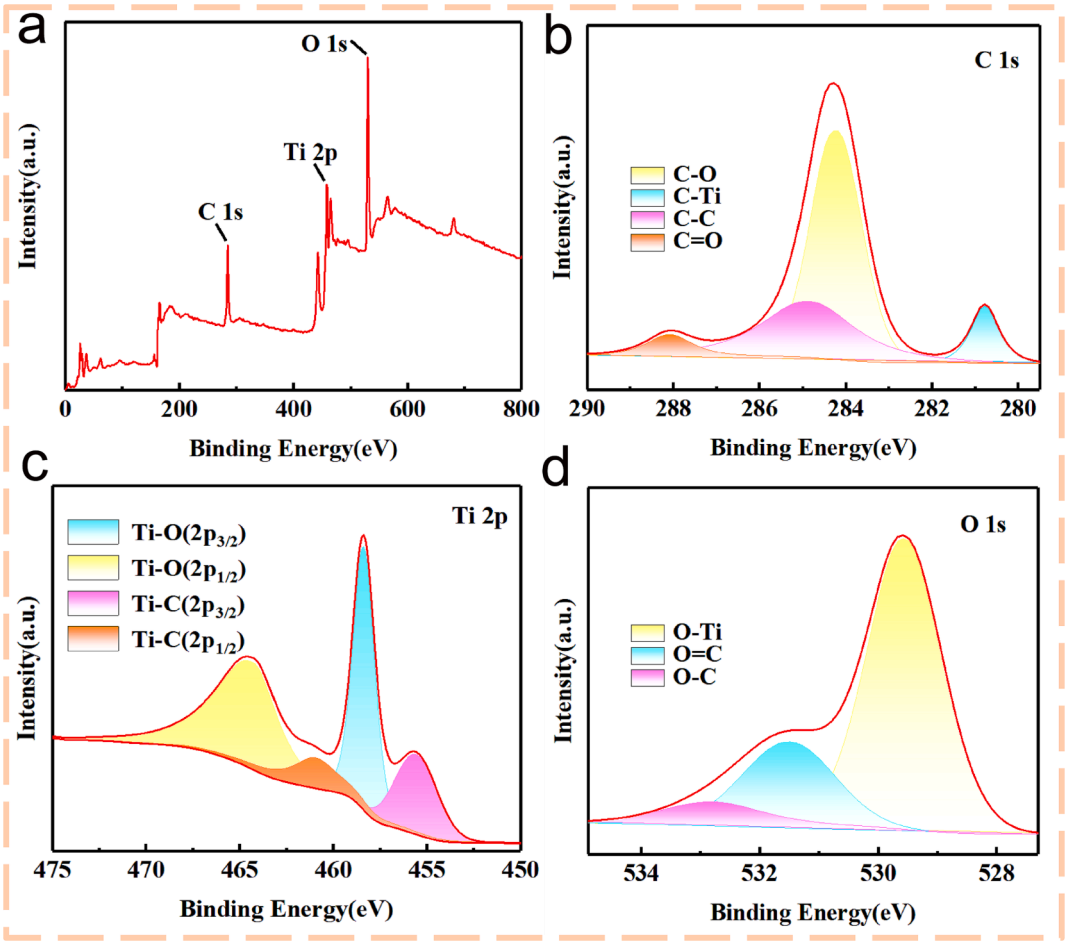

Fig. 4. (a) XPS diagram of $Ti_3C_2T_x$ / TiO_2 prepared with the fluorine-free alkali-assisted hydrothermal method doping with 0.2 mL NaClO aqueous solution; (b) C 1 s, (c) Ti 2p and (d) O 1 s.

532.8 eV, respectively. The results showed that when NaClO was added as an oxidant in the alkali-assisted hydrothermal preparation process, the etched material contains TiO_2.

The electronic structure of $Ti_3C_2T_x/TiO_2$ was further studied by DFT calculation. Fig. 5a was the density of states (DOS) of TiO_2, $Ti_3C_2T_x$ and $Ti_3C_2T_x/TiO_2$. MXene exhibited typical metal characteristics, and its electronic orbit crossed the Fermi level. The synergistic effect of TiO_2 and $Ti_3C_2T_x$ make the composite have stronger interfacial electron interaction than the monomer. By observing the difference charge density along the z-axis in Fig. 5b, there was a significant charge

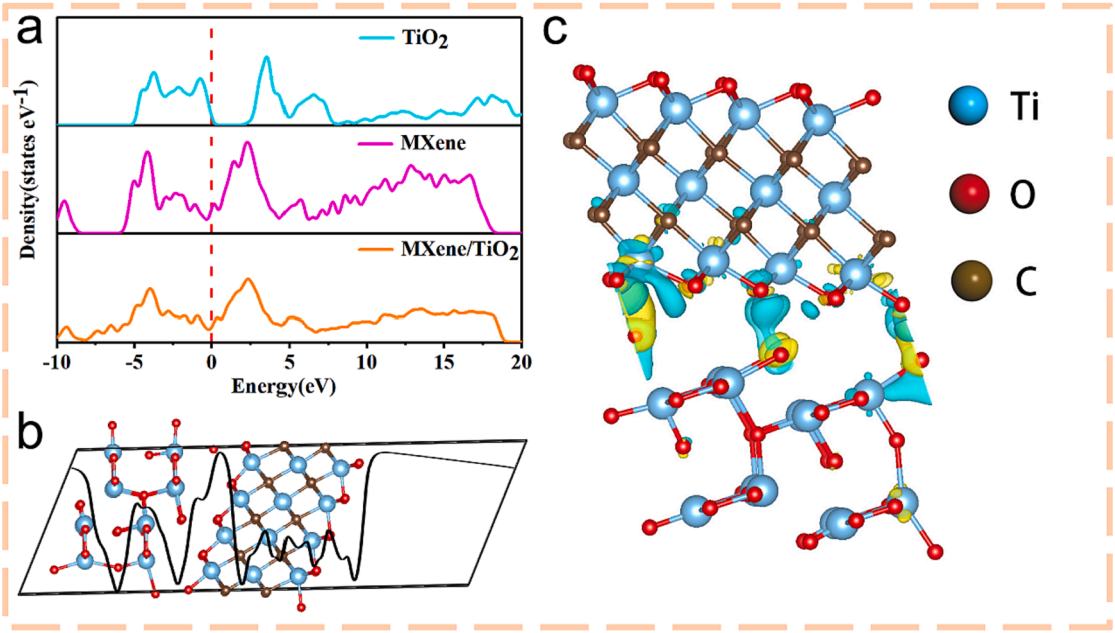

Fig. 5. (a) DOS of TiO_2, MXene and MXene/TiO_2; (b) Ddimensions differential charge density of MXene/TiO_2 along the z-axis; (c) The charge density difference of MXene/TiO_2, yellow represents electron aggregation and blue represents electron dispersion. (For interpretation of the references to colour in this figure legend, the reader is referred to the web version of this article.)

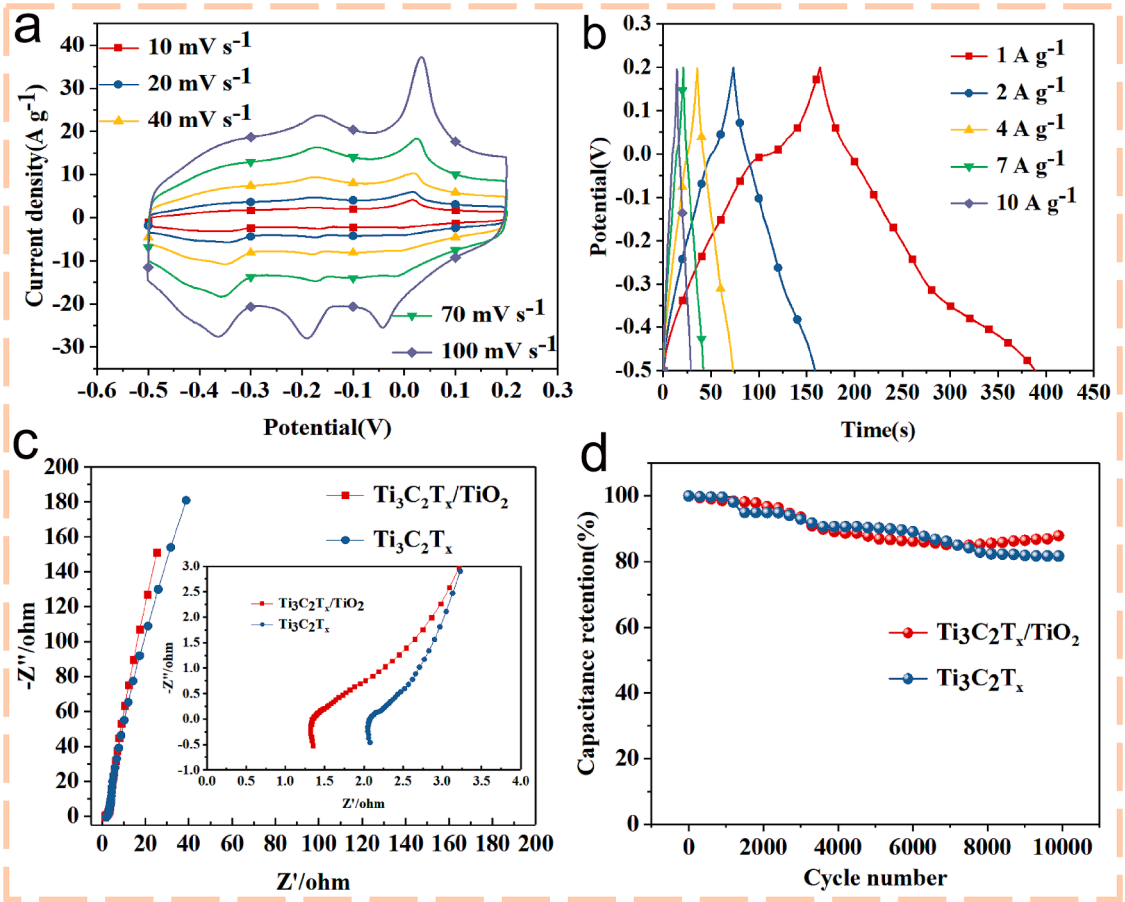

Fig. 6. (a) CV curves of 10 mV, 20 mV, 40 mV, 70 mV, and 100 mV. (b) The constant current charge–discharge curves of the $Ti_3C_2T_x/TiO_2$ composite electrode with 0.2 mL NaClO incorporation in 1 M H_2SO_4 electrolyte and three-electrode system were 1 A/g, 2 A/g, 4 A/g, 7 A/g, 10 A/g, respectively. (c) EIS of $Ti_3C_2T_x/TiO_2$ and $Ti_3C_2T_x$ with incorporation of 0.2 mL NaClO incorporation, and (d) the cyclic stability curves.

redistribution at the heterogeneous interface, which was conducive to the transmission of charge at the interface of the composite material. Fig. 5c showed the interface potential difference of the composite material, it can be found that electrons are aggregated at the yellow and dispersed at the blue. The existence of the potential difference was conducive to the transmission and movement of electrons, indicating that the composite of TiO_2 material can effectively improve the electrical properties of $Ti_3C_2T_x$.

3.2. Electrochemical properties

The electrochemical properties of $Ti_3C_2T_x/TiO_2$ composites prepared by 0.2 mL NaClO aqueous solution were tested in 1 M H_2SO_4 electrolyte using the standard three-electrode system of CHI660E electrochemical workstation. Fig. 6a showed the CV curves of the $Ti_3C_2T_x/TiO_2$ composite electrode with the best reaction time and the best ratio (12 h, 0.2 mL) at 10 mV, 20 mV, 40 mV, 70 mV, and 100 mV. Several CV curves in the figure showed obvious redox peaks, indicating that the material had good pseudocapacitance characteristics. With the increase of scanning speed, the redox peak did not show a significant shift and deformation, indicating that the material had good stability. By observing the constant current charge and discharge curves at current densities of 1 A/g, 2 A/g, 4 A/g, 7 A/g, and 10 A/g in Fig. 6b, and using Formula (2), the highest mass specific capacitance of the prepared $Ti_3C_2T_x/TiO_2$ composite under constant current charge and discharge conditions was calculated to be 321F/g. Electrochemical data of other preparation conditions was shown in Fig. S1 in the supporting information.

The EIS of $Ti_3C_2T_x/TiO_2$ composites and $Ti_3C_2T_x$ materials can further prove the advantages of composites. Fig. 6c was the impedance comparison diagram of the two materials. There was no significant difference in the arc diameter between the two materials in the high frequency region, indicating that the charge transfer resistance was equivalent. The slope of the oblique line in the low frequency region was closely related to the ion diffusion rate in the electrolyte. The slope of the $Ti_3C_2T_x/TiO_2$ composite was significantly higher than that of the pure $Ti_3C_2T_x$ material, indicating that the contact area between the material and the electrolyte was larger, and the ion diffusion rate was better, which was more conducive to improving the conductivity of the material. In addition, the cycle stability test of $Ti_3C_2T_x/TiO_2$ and $Ti_3C_2T_x$ showed that the capacitance retention rate of $Ti_3C_2T_x/TiO_2$ composites was higher than that of $Ti_3C_2T_x$ after 10,000 cycles. As shown in Fig. 6d, the capacitance retention of Ti_3C_2 material was about 81.7 %, while the final capacitance retention of $Ti_3C_2T_x/TiO_2$ composite was 86.4 %, indicating that the TiO_2 composite has higher cycle stability. It was noted that the $Ti_3C_2T_x/TiO_2$ composite gradually increased after 6000 cycles, which was due to the wettability between the electrode material and the electrolyte ions. In summary, the electrical properties of $Ti_3C_2T_x/TiO_2$ composites were better than those of pure $Ti_3C_2T_x$.

4. Conclusion

The fluorine-free $Ti_3C_2T_x/TiO_2$ composite was prepared in situ at a high concentration of NaOH with NaClO. In this composite, the TiO_2 particles prepared in situ were evenly distributed on the surface and between the layers of the material, which effectively curbed the stacking problem between the $Ti_3C_2T_x$ sheets and improved the specific surface area of the material. The prepared electrode in 1 M H_2SO_4 sulfuric acid electrolyte, −0.5–0.2 V voltage window, the highest mass specific capacity can reach 321F/g, and after 10,000 charge–discharge cycles, the capacitance retention rate can still reach 86.4 %, which was higher than that of $Ti_3C_2T_x$ material (81.7 %). The reason was that TiO_2 with excellent pseudocapacitive properties was beneficial to improve the specific capacity of the material, and the composite material prepared by in-situ preparation method, the combination between $Ti_3C_2T_x$ and TiO_2 was closer, ion diffusion and electron conduction were faster. In addition, this in-situ alkali-assisted hydrothermal preparation method effectively reduced unnecessary loss during the experimental process, and did not use a highly toxic and electrochemically inert fluorine-containing solution throughout the experimental process, which provided a new way for the green and efficient preparation of MXene composites.

Declaration of competing interest

The authors declare that they have no known competing financial interests or personal relationships that could have appeared to influence the work reported in this paper.

Acknowledgment

Support by Key R&D plan of Gansu Province (No. 22YF7GA147), Henan Bajian TCM Foundation (2022ZYBJ27), Young and Middle-aged Academic Leaders of Health in Henan Province (2021-024). The authors would like to thank the shiyanjia lab (www. shiyanjia.com) for the TEM, BET, XRD, and XPS test.

Appendix A. Supplementary data

Supplementary data to this article can be found online at https://doi.org/10.1016/j.arabjc.2023.105551.

References

Abdalla, A.M., Abdullah, M.F., Dawood, M.K., Wei, B., Subramanian, Y., Azad, A.T., et al., 2023. Innovative lithium-ion battery recycling: Sustainable process for recovery of critical materials from lithium-ion batteries. J. Storage Mater. 67, 107551.

Ahn, J., Song, Y., Kim, Y.J., Nam, D., Kim, T., Kwak, K., et al., 2023. Redox-active ligand-mediated assembly for high-performance transition metal oxide nanoparticle-based pseudocapacitors. Chem. Eng. J. 455, 140742.

An, N., Shao, Z., Guo, Z., Xin, J., He, Y., Lv, L., et al., 2020. High energy-density supercapacitor based on a novel conjugated poly (1, 5-diaminoanthraquinone)/intercalated graphene composite system. J. Power Sources 475, 228692.

An, N., Guo, Z., Guo, C., Wei, M., Sun, D., He, Y., et al., 2023. A novel COF/MXene film electrode with fast redox kinetics for high-performance flexible supercapacitor. Chem. Eng. J. 458, 141434.

An, N., Li, W., Shao, Z., Zhou, L., He, Y., Sun, D., et al., 2023. Graphene oxide coated polyaminoanthraquinone@MXene based flexible film electrode for high-performance supercapacitor. J. Storage Mater. 57, 106180.

Bagal, I.V., Chodankar, N.R., Waseem, A., Ali Johar, M., Patil, S.J., Abdullah, A., et al., 2021. CF_4 plasma-treated porous silicon nanowire arrays laminated with MnO_2 nanoflakes for asymmetric pseudocapacitors. Chem. Eng. J. 419, 129515.

Cao, L., Wang, C., Huang, Y., 2023. Structure optimization of graphene aerogel-based composites and applications in batteries and supercapacitors. Chem. Eng. J. 454, 140094.

Chen, G.Z., 2021. Linear and non-linear pseudocapacitances with or without diffusion control. Prog. Nat. Sci.: Mater. Int. 31 (6), 792–800.

Chen, C., Gao, Y., Wang, X., 2023. Ion intercalation process in MXene pseudocapacitors with aqueous and non-aqueous electrolytes. In: Encyclopedia of Materials: Electronics. Oxford; Academic Press, pp. 237–249.

Chowdhury, A., Shukla, R., Bhattacharyya, K., Tyagi, A.K., Chandra, A., Grover, V., 2023. Electrochemical performance of K+ -intercalated MnO2 nano-cauliflowers and their Na-ion-based pseudocapacitors. Mater. Sci. Eng. B 295, 116581.

Das, K., Majumdar, D., 2022. Prospects of MXenes/graphene nanocomposites for advanced supercapacitor applications. J. Electroanal. Chem. 905, 115973.

Fei, Z., Su, Y., Zha, Y., Zhao, X., Meng, Q., Dong, P., et al., 2023. Selective lithium extraction of cathode materials from spent lithium-ion batteries via low-valent salt assisted roasting. Chem. Eng. J. 464, 142534.

Gao, B., Li, X., Ma, Y., Cao, Y., Hu, Z., Zhang, X., et al., 2015. MnO_2-TiO_2/C nanocomposite arrays for high-performance supercapacitor electrodes. Thin Solid Films 584, 61–65.

Grover, S., Kadyan, P., Sharma, S., Sharma, K., Sharma, R.K., 2023. Synthesis and characterization of polyaniline nanotube supported nanocomposite of RuO_2 as electrode material for application in supercapacitor device. Materialia 28 (101732).

Grygorchak, I., Shvets, R., Kityk, I.V., Kityk, A.V., Wielgosz, R., Hryhorchak, O., et al., 2019. Photosensitive carbon supercapacitor: cavitated nanoporous carbon from iodine doped β–cyclodextryn. Physica E 108, 164–168.

Halim, J., Lukatskaya, M.R., Cook, K.M., Lu, J., Smith, C.R., Näslund, L.-Å., May, S.J., Hultman, L., Gogotsi, Y., Eklund, P.J.C.o.M., 2014. Transparent conductive two-dimensional titanium carbide epitaxial thin films. Chem. Mater. 26 (7), 2374–2381.

Han, S., Park, S., Yi, S.-H., Im, W.B., Chun, S.-E., 2020. Effect of potential and current on electrodeposited MnO_2 as a pseudocapacitor electrode: Surface morphology/chemistry and stability. J. Alloys Compd. 831, 154838.

He, Z.-K., Lu, Y., Zhao, C., Zhao, J., Gao, Z., Song, Y.-Y., 2021. Surface-charge regulated TiO_2 nanotube arrays as scaffold for constructing binder-free high-performance supercapacitor. Appl. Surf. Sci. 567, 150832.
Hung, P., Zhang, H., Lin, H., Guo, Q., Lau, K., Jia, B., 2022. Specializing liquid electrolytes and carbon-based materials in EDLCs for low-temperature applications. J. Energy Chem. 68, 580–602.
Karimi, F., Korkmaz, S., Karaman, C., Karaman, O., Afşin, K.İ., 2022. Engineering of GO/MWCNT/RuO2 ternary aerogel for high-performance supercapacitor. Fuel 329, 125398.
Khajonrit, J., Sichumsaeng, T., Kalawa, O., Chaisit, S., Chinnakorn, A., Chanlek, N., et al., 2022. Mangosteen peel-derived activated carbon for supercapacitors. Prog. Nat. Sci.: Mater. Int. 32 (5), 570–578.
Lakra, R., Kumar, R., Kumar, S., Thatoi, D., Soam, A., 2023. Synthesis of TiO_2 nanoparticles as electrodes for supercapacitor. Mater. Today:. Proc. 74, 863–866.
Li, J., Ao, J., Zhong, C., Yin, T., 2021. Three-dimensional nanobranched TiO_2-carbon nanotube for high performance supercapacitors. Appl. Surf. Sci. 563, 150301.
Li, T., Yao, L., Liu, Q., Gu, J., Luo, R., Li, J., Yan, X., Wang, W., Liu, P., Chen, B., Zhang, W., Abbas, W., Naz, R., Zhang, D., 2018. Fluorine-free synthesis of high-purity Ti3C2Tx (T=OH, O) via alkali treatment. Angew. Chem. Int. Ed. 57 (21), 6115–6119.
Lichchhavi, K.S., Srivastava, A.K., Jha, S.K., 2023. Elucidation of intercalation-pseudocapacitor mechanism in Binder-free Bi_2S_3@Ni foam electrodes towards high-performance supercapattery. Electrochim. Acta 456 (142438).
Liu, B., Cao, Z., Yang, Z., Qi, W., He, J., Pan, P., et al., 2022. Flexible micro-supercapacitors fabricated from MnO_2 nanosheet/graphene composites with black phosphorus additive. Prog. Nat. Sci.: Mater. Int. 32 (1), 10–19.
Liu, H., Liu, Y., Xu, D., Chen, L., Guo, W., Gu, T., et al., 2022. 3D Cross-linked $Ti_3C_2T_x$-Ca-SA films with expanded $Ti_3C_2T_x$ interlayer spacing as freestanding electrode for all-solid-state flexible pseudocapacitor. J. Colloid Interface Sci. 610, 295–303.
Lv, H., Fan, C., Xu, X., Zhao, C., Long, J., 2023. Rational design to manganese-doped amorphous tetra-metallic oxides as efficient catalysts for LiO_2 batteries. Solid State Ion. 391, 116146.
Mahala, S., Khosravinia, K., Kiani, A., 2023. Unwanted degradation in pseudocapacitors: Challenges and opportunities. J. Storage Mater. 67, 107558.
Manuraj, M., Chacko, J., Narayanan Unni, K.N., Rakhi, R.B., 2020. Heterostructured MoS_2-RuO_2 nanocomposite: a promising electrode material for supercapacitors. J. Alloys Compd. 836, 155420.
Naguib, M., Kurtoglu, M., Presser, V., Lu, J., Niu, J., Heon, M., Hultman, L., Gogotsi, Y., Barsoum, M.W.J.A.m., 2011. Two-dimensional nanocrystals produced by exfoliation of Ti3AlC2. Adv. Mater. 23 (37), 4248–4253.
Natu, V., Pai, R., Sokol, M., Carey, M., Kalra, V., Barsoum, M.W.J.C., 2020. 2D $Ti_3C_2T_z$ MXene synthesized by water-free etching of Ti_3AlC_2 in polar organic solvents. Chem 6 (3), 616–630.
Panda, S., Deshmukh, K., Khadheer Pasha, S.K., Theerthagiri, J., Manickam, S., Choi, M. Y., 2022. MXene based emerging materials for supercapacitor applications: Recent advances, challenges, and future perspectives. Coord Chem Rev 462, 214518.
Qu, W., Hu, P., Liu, J., Jin, H., Wang, K., 2022. Lignin-based carbon fiber: A renewable and low-cost substitute towards featured fiber-shaped pseudocapacitor electrodes. J. Clean. Prod. 343, 131030.
Seo, S.W., Ahn, W.J., Kang, S.C., Im, J.S., 2023. Investigation of electrical conductivity based on porous hollow carbon black for EDLC. Inorg Chem Commun 151, 110571.
Simon, S.M., P, V.P., S, M.S., Chandran, A., George, G., Barmiah, E.K., et al., 2023. Development and characterizations of Ag nanoparticles decorated TiO_2-ZrO_2 coatings as electrode material for supercapacitors. Results Surfaces Interf. 10 (100098).
Sun, J., Bi, H., 2012. Pickering emulsion fabrication and enhanced supercapacity of graphene oxide-covered polyaniline nanoparticles. Mater. Lett. 81, 48–51.
Sun, J., Farid, M.U., Boey, M.W., Sato, Y., Chen, G., An, A.K., 2023. MXene-PVA-TiO_2-based photothermal-catalytic membrane with high structural stability for efficient desalination and photodegradation. Chem. Eng. J. 468, 143744.
Sun, S., Wang, L., Xu, H., 2022. Characteristics of graphite oxide membranes with different thickness by low temperature thermal reduction for aqueous EDLC electrodes and hot activation phenomenon. Mater. Res. Bull. 154, 111927.
Thangappan, R., Arivanandhan, M., Dhinesh Kumar, R., Jayavel, R., 2018. Facile synthesis of RuO_2 nanoparticles anchored on graphene nanosheets for high performance composite electrode for supercapacitor applications. J. Phys. Chem. Solids 121, 339–349.
Tovar-Martinez, E., Sanchez-Rodriguez, C.E., Sanchez-Vasquez, J.D., Reyes-Reyes, M., López-Sandoval, R., 2023. Synthesis of carbon spheres from glucose using the hydrothermal carbonization method for the fabrication of EDLCs. Diamond Relat. Mater. 136, 110010.
Waris, H.A., Abdulaziz, F., Latif, S., Alanazi, A., Sultana, S., et al., 2023. Microwave assisted green synthesis of high capacitive TiO_2 doped rGO nanosheets for supercapacitor applications. Mater. Sci. Eng. B 291 (116367).
Wodyk, S., Wieczorek, M., Witaszek, P., Poliszkiewicz, R., 2023. Design and control of the hybrid lithium-ion/lead–acid battery. Energy Rep. 9, 106–115.
Wu, H., Li, D., Zhu, X., Yang, C., Liu, D., Chen, X., et al., 2014. High-performance and renewable supercapacitors based on TiO_2 nanotube array electrodes treated by an electrochemical doping approach. Electrochim. Acta 116, 129–136.
Xiao, Y., Liu, Y., Liu, F., Han, P., Qin, G., 2020. Wearable pseudocapacitor based on porous MnO_2 composite. J. Alloys Compd. 813, 152089.
Yang, Y., Wang, R., Shen, Z., Yu, Q., Xiong, R., Shen, W., 2023. Towards a safer lithium-ion batteries: a critical review on cause, characteristics, warning and disposal strategy for thermal runaway. Adv. Appl. Energy 11, 100146.
Ye, F., Xu, B., Chen, R., Li, R., Chang, G., 2023. A high performance flexible cotton-based supercapacitor prepared by in-situ polyaniline and MXene coating. J. Storage Mater. 62, 106803.
Zeng, C., Duan, C., Guo, Z., Liu, Z., Dou, S., Yuan, Q., et al., 2022. Ultrafastly activated needle coke as electrode material for supercapacitors. Prog. Nat. Sci.: Mater. Int. 32 (6), 786–792.
Zhang, K., Cen, Z., Yang, F., Xu, K., 2021. Rational construction of $NiCo_2O_4$@Fe_2O_3 core-shell nanowire arrays for high-performance supercapacitors. Prog. Nat. Sci.: Mater. Int. 31 (1), 19–24.
Zhang, B., Liu, Q., Xu, K., Zou, R., Wang, C., 2022. Electrochemical energy storage application of CuO/CuO@Ni–$CoMoO_4$·0.75H_2O nanobelt arrays grown directly on Cu foam. Prog. Nat. Sci.: Mater. Int. 32 (2), 163–170.
Zhang, J., Wang, Y., Qin, Y., Yu, C., Cui, L., Shu, X., et al., 2017. A facile one-step synthesis of Mn_3O_4 nanoparticles-decorated TiO_2 nanotube arrays as high performance electrode for supercapacitors. J. Solid State Chem. 246, 269–277.
Zhao, Z., Wu, X., Luo, C., Wang, Y., Chen, W., 2022. Rational design of $Ti_3C_2Cl_2$ MXenes nanodots-interspersed MXene@NiAl-layered double hydroxides for enhanced pseudocapacitor storage. J. Colloid Interface Sci. 609, 393–402.
Zhao, C., Zhang, Y., Nie, K., Yi, L., Li, B., Yuan, Y., et al., 2023. Recent advances in design and engineering of MXene-based heterostructures for sustainable energy conversion. Appl. Mater. Today 32, 101841.
Zheng, X., Wang, Y., Nie, W., Wang, Z., Hu, Q., Li, C., et al., 2022. Elastic polyaniline nanoarrays/MXene textiles for all-solid-state supercapacitors and anisotropic strain sensors. Compos. A Appl. Sci. Manuf. 158, 106985.